Atmos. Chem. Phys. Discuss., 14, 5929–5961, 2014
www.atmos-chem-phys-discuss.net/14/5929/2014/
doi:10.5194/acpd-14-5929-2014

Atmospheric Chemistry and Physics Discussions

Molecular corridors represent the multiphase chemical evolution of secondary organic aerosol

M. Shiraiwa[1], T. Berkemeier[1], K. A. Schilling-Fahnestock[2], J. H. Seinfeld[2], and U. Pöschl[1]

[1]Multiphase Chemistry Department, Max Planck Institute for Chemistry, 55128 Mainz, Germany
[2]Division of Chemistry and Chemical Engineering, California Institute of Technology, Pasadena, CA91125, USA

Received: 21 February 2014 – Accepted: 25 February 2014 – Published: 6 March 2014

Correspondence to: M. Shiraiwa (m.shiraiwa@mpic.de)

Published by Copernicus Publications on behalf of the European Geosciences Union.

Abstract

The dominant component of atmospheric organic aerosol is that derived from the oxidation of volatile organic compounds (VOCs), so-called secondary organic aerosol (SOA). SOA consists of a multitude of organic compounds, only a small fraction of which has historically been identified. Formation and evolution of SOA is a complex process involving coupled chemical reaction and mass transport in the gas and particle phases. Current SOA models do not embody the full spectrum of reaction and transport processes nor do they identify the dominant rate-limiting steps in SOA formation. The recent advent of soft ionization mass spectrometry methods now facilitates a more complete molecular identification of SOA than heretofore possible. Based on such novel measurements, we show here that the chemical evolution of SOA from a variety of VOC precursors adheres to characteristic "molecular corridors" with a tight inverse correlation between volatility and molar mass. Sequential and parallel reaction oxidation and dimerization pathways progress along these corridors through characteristic regimes of reaction-, diffusion-, or accommodation-limited multiphase chemical kinetics that can be classified according to reaction location, degree of saturation, and extent of heterogeneity of gas and particle phases. These molecular corridors constrain the properties of unidentified products and reaction pathways and rates of SOA evolution, thereby facilitating the further development of aerosol models for air quality and climate.

1 Introduction

Organic aerosol is ubiquitous in the atmosphere and its major component is secondary organic aerosol (SOA) (Jimenez et al., 2009). Reaction of atmospheric VOCs with oxidants such as OH, O_3, and NO_3 initiate the formation of semi-volatile organic compounds (SVOCs), which can undergo further gas-phase oxidation to form low-volatility organic compounds (LVOCs) that will preferentially partition into the particle phase

ACPD
14, 5929–5961, 2014

(Kroll and Seinfeld, 2008; Hallquist et al., 2009; Donahue et al., 2012). A fraction of the SVOCs partitions into the particle phase, wherein they can be transformed into LVOCs such as oligomers and other high molecular mass compounds (Jang et al., 2002; Kalberer et al., 2006; Ervens et al., 2011; Ziemann and Atkinson, 2012; Shiraiwa et al., 2013a). Some portion of the LVOCs can be transformed back to (semi-)volatile compounds or CO/CO_2 by fragmentation reactions triggered by OH or other oxidants in the particle phase (Kroll and Seinfeld, 2008; Jimenez et al., 2009). SOA partitioning is also affected by particle-phase state, non-ideal thermodynamic mixing and morphology (Chang and Pankow, 2006; Zuend and Seinfeld, 2012; Shiraiwa et al., 2013b).

SOA consists of a myriad of organic compounds of which only 10–30 % have been identified (Goldstein and Galbally, 2007). With the advent of soft ionization mass spectrometry methods, it is becoming possible to identify the dominant fraction of the compounds constituting SOA (Kalberer et al., 2006; Williams et al., 2010; Vogel et al., 2013). This powerful information opens up a window onto the pathways of SOA formation and aging that was heretofore unavailable. Taking advantage of such data here we present a new 2-D map for SOA evolution of molar mass vs. volatility, which can be linked to kinetic regimes and reaction pathways of formation and aging of SOA that is currently poorly constrained and a major limitation in the understanding and prediction of atmospheric aerosol effects.

2 Identification of SOA oxidation products

Figure 1 shows 2-D maps involving molar mass (or molecular weight) vs. volatility (or saturation mass concentration) for major oxidation products of biogenic SOA derived from (a) isoprene (Surratt et al., 2006, 2010), (b) α-pinene (Docherty et al., 2005; Zuend and Seinfeld, 2012), and (c) limonene (Jaoui et al., 2006; Kundu et al., 2012), and anthropogenic SOA from C_{12} alkanes, (d, e) dodecane (Yee et al., 2012), (f, g) cyclododecane, and (h, i) hexylcyclohexane. The composition of C_{12} alkanes at low- and high-NO conditions was obtained using direct analysis in real-time – time-of-flight

ACPD
14, 5929–5961, 2014

and ion trap mass spectrometry (JEOL DART-AccuToF; Thermo Fisher LTQ ion trap MS) (see Appendix A). SOA compounds identified include alcohol, ketone, aldehyde, hydroxycarbonyl, organic hydroperoxide and nitrate, which are generated in the gas phase (open markers), as well as dihydrofuran, furan, ether, ester, peroxyhemiacetal, hemiacetal, dimer, and imine, which are likely particle-phase products (Ziemann and Atkinson, 2012) (solid markers). The markers in Fig. 1 are color-coded with atomic O : C ratio.

Generally, volatility decreases and molar mass increases with chemical aging of SOA both in the gas and particle phases. Consequently, molar mass of oxidation products tightly correlates with volatility with high coefficient of determination (R^2). The 95 % confidence prediction intervals (dashed lines in Fig. 1) can be regarded as molecular corridors within which additional unidentified oxidation products are likely to fall. The average slope of the fitted dotted lines for all SOA systems in Fig. 1 is 20 (±4), indicating that product volatility decreases one order of magnitude when molar mass increases by $\sim 20\,\mathrm{g\,mol^{-1}}$.

3 Kinetic regimes for SOA formation

Traditionally, SOA formation has been modeled based on instantaneous gas-particle equilibrium partitioning, implicitly assuming that the rate-limiting step for SOA formation is gas-phase reaction (Pankow, 1994; Hallquist et al., 2009). It is now known that SOA formation is more complex than previously thought, potentially tightly coupled through a sequence of mass transport and chemical reaction (Shiraiwa et al., 2013a) (Fig. 2a). Recently, Berkemeier et al. (2013) provided a conceptual framework within which kinetic regimes of vapor uptake and heterogeneous reactions in atmospheric aerosols and clouds can be assigned. By extending this framework to represent the complex interplay of gas- and particle-phase reactions in SOA formation and evolution, a systematic classification of the rate-limiting processes emerges for analysis and interpretation of laboratory chamber data and ambient measurements, and for com-

ACPD
14, 5929–5961, 2014

parison of experimental results with theoretical predictions. Different types of kinetic behavior can be characterized by three basic criteria as detailed in the Appendix B: (1) the location of the chemical reaction leading to SOA formation or aging (gas phase, particle surface, particle bulk), (2) the saturation ratio of the reactants (ratio of ambient concentration to saturation concentration), and (3) the extent of spatial heterogeneity of the gas and particle phases (concentration gradients). The corresponding regimes and limiting cases can be visualized on a "kinetic cuboid", in which each axis corresponds to one of the three classification properties (Fig. 2b). In Fig. 2, "G", "S", and "B" indicate the predominant reaction location: gas phase, particle surface, or particle bulk, respectively. A subscript denotes the rate-limiting process for SOA formation and aging: "rx" indicates chemical reaction; "bd" indicates bulk diffusion; "α" indicates mass accommodation; "gd" indicates gas-phase diffusion. The left side of the cuboid can be regarded as a particle-phase reaction regime (SB) that comprises eight limiting cases of kinetic behavior (B_{rx}, S_{rx}, B_{bd}, S_{bd}, B_{α}, S_{α}, B_{gd}, S_{gd}); the right side constitutes a gas-phase reaction regime (G) with four specific limiting cases (G_{rx}, G_{bd}, G_{α}, G_{gd}). Depending on atmospheric composition and reaction conditions, which vary widely in space and time, the chemical evolution of organic compounds and SOA particles can progress through these regimes.

4 Molecular corridors

Figure 3 shows the molecular corridors of molar mass vs. volatility encompassing six SOA systems in Fig. 1 as well as products of aqueous-phase glyoxal oxidation (Lim et al., 2010), with totally 872 identified oxidation products. Gas-phase functionalization generally leads to a slight increase in molar mass, whereas fragmentation leads to a substantial increase of volatility and decrease of molar mass. Thus, gas-phase oxidation products are confined to the lower right area in the 2-D space. Kinetic regimes associated with the generation of these products are indicated in Fig. 3. Early generation oxidation products ($C_0 > 10\,\mu g\,m^{-3}$) tend to fall into the gas-phase reaction lim-

ACPD
14, 5929–5961, 2014

iting case G_{rx}, as the gas-particle equilibration timescale of such products is of order seconds (Shiraiwa and Seinfeld, 2012) (see Appendices C and D). Later generation semi-volatile and low volatility products do not necessarily adhere to equilibrium partitioning (Vogel et al., 2013). These observations are consistent with kinetic limitations of gas-to-particle transfer associated with mass accommodation (G_{α}) or retarded bulk diffusion (G_{bd}), when organic particles adopt amorphous solid or semi-solid states (Shiraiwa et al., 2011; Vaden et al., 2011; Kuwata and Martin, 2012; Shiraiwa and Seinfeld, 2012; Renbaum-Wolff et al., 2013).

The particle-phase reaction regime (SB) often involves two or more species leading to formation of low volatility, high molar mass compounds (Ziemann and Atkinson, 2012), which tend to lie in the upper left area in the 2-D space. Exceptions are dihydrofurans and furans, which are semi-volatile particle-phase products in dodecane and cyclododecane SOA (Yee et al., 2012; Ziemann and Atkinson, 2012). The formation of particle-phase products is likely to be limited by reaction or diffusion in the particle bulk, as second-order rate coefficients for dimer formation are relatively low ($< 10\,M^{-1}\,s^{-1}$) (Ziemann and Atkinson, 2012). Note that particle-phase reactions can also be limited by gas-to-particle mass transfer (e.g., accommodation, supply of reactive gases into the particle), when they are sufficiently fast, such as catalyzed by acids (Jang et al., 2002; Surratt et al., 2010). As SOA oxidation products migrate progressively upward and to the left in the molecular corridor, the kinetic regime of SOA growth may evolve from G_{rx} over G_{α} or G_{bd} to SB. Thus, even though equilibrium gas-particle partitioning may hold for early generation oxidation products, SOA formation may become kinetically limited for later generation gas-phase and particle-phase products (Riipinen et al., 2011; Perraud et al., 2012; Shiraiwa et al., 2013a).

The dashed lines in Fig. 3 represent *n*-alkanes C_nH_{2n+2} and long-chain sugar alcohols $C_nH_{2n+2}O_n$. SOA oxidation products generally have O : C ratio of 0–1 (Jimenez et al., 2009), falling between these lines. The molecular corridor seems to be split into two corridors based on O : C ratio. Many early generation gas-phase oxidation products and high molar mass compounds, including dimers and peroxyhemiacetals, lie close

ACPD
14, 5929–5961, 2014

to the C_nH_{2n+2} line with low O : C ratio (low O : C compounds; LOC); whereas later generation oxidation products have high O : C ratio and lie close to the $C_nH_{2n+2}O_n$ line (high O : C compounds; HOC). Aqueous phase processing of glyoxal (Lim et al., 2010; Ervens et al., 2011) and autoxidation (inter- and intramolecular hydrogen abstraction by peroxy radicals) (Crounse et al., 2013) represent, for example, efficient pathways for the formation of HOC compounds. As shown in Fig. 1, any particular precursor system generally follows either LOC or HOC behavior; interestingly, hexylcyclohexane SOA populates regions in both corridors.

An abundance of high molecular weight SOA compounds (e.g., oligomers) results in high average molar mass for the biogenic systems of isoprene and α-pinene (Kalberer et al., 2006) as well as the anthropogenic C_{12} alkanes (Fig. 1). Figure 3 shows that the region of 250–300 g mol^{-1} appears to be a threshold between gas- and particle-phase products (excepting furans and glyoxal products). Thus, placing identified compounds within the molecular corridor facilitates estimation of the relative contributions of gas- vs. particle-phase routes to SOA mass. The relatively high average molar mass for laboratory-generated SOA points to the importance of particle-phase chemistry. Relatively lower molar masses reported for ambient organic aerosols in Riverside, California (Williams et al., 2010) and Hyytiälä, Finland (Vogel et al., 2013) indicate that both gas- and particle-processes are comparably important in their formation.

Molar mass correlates also with the glass transition temperature of organic compounds, wherein the molecular O : C ratio itself is of secondary importance: the higher the molar mass, the higher the glass transition temperature (Koop et al., 2011). An elevated glass transition temperature is indicative of a semi-solid or amorphous solid state (Virtanen et al., 2010; Koop et al., 2011; Renbaum-Wolff et al., 2013). SOA composition as represented in molecular corridor allows one to infer the regime, in which particles are likely to become highly viscous. For example, recent experiments have shown an order of magnitude increase in the viscosity of oleic acid particles upon reaction with ozone owing to formation of oligomers (Hosny et al., 2013).

ACPD
14, 5929–5961, 2014

In summary, presenting identified SOA products in a molecular corridor encapsulates fundamental aspects of SOA formation and aging: volatility, molar mass, O : C ratio, and phase state. Such a representation can be used to constrain/predict the properties of unidentified SOA oxidation products. The kinetic regimes, within which SOA evolution is occurring along the molecular corridor, facilitate the specification of the rate of progression to higher generation products. Thus, molecular corridors may serve as a basis for compact representation of SOA formation and aging in regional and global models of climate and air quality.

Appendix A

Product analysis of alkane SOA

Photo-oxidation and subsequent SOA formation of *n*-dodecane, cyclododecane, and hexylcyclohexane was conducted in the 28 m^3 Teflon reactors in the Caltech Environmental chamber (Yee et al., 2012; Loza et al., 2013). Aqueous H_2O_2 solution was evaporated into the chamber as the OH source, followed by the atomization of an aqueous ammonium sulfate solution generating seed particles, which were subsequently dried. Experiments were conducted under low-NO conditions, in which alkyl peroxy radicals (RO_2) react primarily with HO_2, and under high-NO conditions, in which RO_2 react primarily with NO (Loza et al., 2013).

SOA particles were collected on Teflon filters (Pall Life Sciences, 47 mm, 1.0 µm pore size). Off-line analysis of collected particles was conducted by solvent extraction and gas chromatography time-of-flight mass spectrometry (GC-TOF-MS, GCT Premier, Waters) and GC/ion trap mass spectrometry (Varian Saturn 2000, Agilent), and by direct analysis in real time (DART)-time-of-flight and ion trap mass spectrometry (DART-AccuToF, JEOL USA; Caltech Mini-DART; LTQ, Thermo Fisher).

The average molar mass of SOA was estimated by taking the sum of the product of the percent relative concentration of each compound with respect to the internal stan-

ACPD
14, 5929–5961, 2014

dard (dibutyl phthalate present in each filter) by each compound's molar mass. The relative concentration for each compound was obtained through the relationship of ion current intensity and concentration for DART-MS. In DART analysis, ion current intensity (I) is proportional to the concentration (C), vapor pressure (P_{vap}) and proton affinity (A): $I = AP_{vap}C$. This equation is written for both the analyte and the internal standard and then the ratio was calculated, which allows for the cancellation of the proton affinity term. Analyte vapor pressures were estimated by using proposed structures based on HR-MS data-derived formulae and known mechanisms with the EVAPORATION (Estimation of vapor pressure of organics, accounting for temperature, intramolecular, and non-additivity effects) model (Compernolle et al., 2011). When rewritten to solve for the relative concentration of the analyte with respect to the concentration of the internal standard, the equation becomes:

$$\frac{C_A}{C_{IS}} = \frac{P_{vap,IS}}{P_{vap,A}} \frac{I_A}{I_{IS}} \quad \text{(A1)}$$

Table A1 lists the number of identified oxidation products, average molar mass, and the slope of the fitted line in Fig. 2. The identified gas- and particle-phase oxidation products by biogenic precursors of isoprene (Surratt et al., 2006, 2010), α-pinene (Docherty et al., 2005; Zuend and Seinfeld, 2012), and limonene (Jaoui et al., 2006; Kundu et al., 2012) were taken from the literature, vapor pressures of which were estimated by the EVAPORATION (Estimation of vapor pressure of organics, accounting for temperature, intramolecular, and non-additivity effects) model (Compernolle et al., 2011).

Atomic O : C ratio vs. volatility is used to represent formation and aging of SOA (Jimenez et al., 2009; Donahue et al., 2011). By analogy to Figs. 1 and 3, major oxidation products are shown in Figs. A1 and A2 for SOA precursors including (a) isoprene (Surratt et al., 2006, 2010), (b) α-pinene (Docherty et al., 2005; Zuend and Seinfeld, 2012), and (c) limonene (Jaoui et al., 2006; Kundu et al., 2012); and anthropogenic precursors of (d, e) dodecane (Yee et al., 2012), (f, g) cyclododecane, and (h, i) hexyl-

ACPD
14, 5929–5961, 2014

cyclohexane at low- and high-NO conditions. The markers are color coded by molar mass.

Upon gas-phase oxidation, volatility decreases and O : C ratio increases, leading to a linear correlation in O : C ratio vs. volatility for gas-phase oxidation products. Particle-phase products, however, exhibit generally lower volatility and O : C ratio as compared to gas-phase oxidation products. Consequently, the overall correlation between O : C ratio and volatility for the full spectrum of SOA products has a low coefficient of determination and wide prediction interval (Fig. A1, Table A1). Figure A2 shows the summary of O : C ratio vs. volatility, including oxidation products from the aqueous-phase chemistry of glyoxal (Lim et al., 2010), along with possible kinetic regimes and limiting cases. The oxidation products cover almost the full area in this 2-D space. Clear trend is found that volatile compounds have low molar mass, whereas low volatility compounds with low O : C ratio have high molar mass.

Appendix B

Kinetic regimes for SOA formation

Figure A3 shows a classification scheme for kinetic regimes and limiting cases for SOA formation and aging. Note that the term *limiting case* is reserved for a system that is governed by a single, clearly defined limiting process; the term *kinetic regime* designates a system that is governed by a few (often only one or two) clearly defined rate-limiting processes (Berkemeier et al., 2013). The classification within the particle phase regime (right-hand side of Fig. 2) is explained in detail by Berkemeier et al. (2013). In this study, the gas-phase regime (left-hand side of Fig. 2) extends the classification scheme to SOA formation. The cases of limiting behavior arise from three criteria that are fundamental to formation and partitioning of an oxidation product: (1) the location (gas phase, particle surface, particle bulk) of the reaction leading to SOA formation, (2) the species' saturation ratio (ratio of ambient concentration to saturation concen-

ACPD
14, 5929–5961, 2014

tration) of the oxidation products, and (3) the extent of spatial heterogeneity of the gas and particle phases. Identifying kinetic regimes and limiting cases can be facilitated by an aerosol model, such as the kinetic multi-layer model for gas-particle interactions (KM-GAP) that explicitly resolves mass transport and chemical reactions in the gas and particle phases (Shiraiwa et al., 2012).

B1 Criterion 1: reaction location (gas vs. surface vs. bulk)

Where does formation of oxidation products that contribute to SOA mass predominantly occur, gas phase, particle surface or particle bulk? A two-pronged criterion can be developed. The first sub-criterion evaluates the relative contribution of gas- vs. particle-phase chemistry. The gas- vs. particle-phase contribution ratio (GPCR) can be defined as ratio of the production rate of the oxidation product in the gas phase (P^g) to the total production rate in gas and particle phases ($P^g + P^p$):

$$\mathrm{GPCR} = P^g/(P^g + P^p) \tag{B1}$$

As GPCR approaches unity, an oxidation product is produced primarily in the gas phase; and as GPCR approaches zero, it is primarily produced in the particle phase.

If particle-phase chemistry dominates (GPCR $\approx$ 0), the surface to total particle phase contribution ratio (STCR) is used to assess the extent to which production occurs predominantly at the surface or in the bulk. STCR can be calculated using the production rate of the oxidation product at the surface (P^s) and in the particle bulk (P^b):

$$\mathrm{STCR} = P^s/(P^s + P^b) \tag{B2}$$

If the particle-phase reaction primarily occurs at the surface, STCR approaches unity; and STCR approaches zero if the reaction occurs primarily in the bulk.

B2 Criterion 2: saturation ratio

Is mass transfer of an oxidation product through the gas or into the particle phase limiting SOA growth? After determination of the reaction location, this criterion further

ACPD
14, 5929–5961, 2014

classifies the system based on the abundance of oxidation products at the particle surface vs. in the near-surface bulk.

In the gas-phase regime, the surface saturation ratio (SSR) can be used to judge the extent to which kinetic limitation of mass transport occurs in the gas phase. With this parameter, the surface concentration of an oxidation product Z, $[Z]_s$, is compared to its surface saturation concentration $[Z]_{s,\,sat}$. In the absence of reaction or diffusion into the bulk, $[Z]_{s,\,sat}$ is determined by the gas-phase concentration of Z, $[Z]_g$, and the rates of adsorption and desorption k_a and k_d: $[Z]_{s,\,sat} = k_a/k_d[Z]_g$ (Pöschl et al., 2007; Berkemeier et al., 2013). The SSR is defined as the ratio of $[Z]_s$ to its saturation concentration at adsorption equilibrium:

$$\mathrm{SSR} = [Z]_s/[Z]_{s,\,sat} \tag{B3}$$

The numerical interpretation of SSR is: (1) As SSR approaches zero, the surface is starved of Z, and the system is limited by mass transfer either by gas-phase diffusion (G_{gd} limiting case) or surface accommodation (G_{α} limiting case). As SSR approaches unity, the surface is adequately supplied with Z and the system can be limited by production of Z in the gas phase (G_{rx} limiting case) or mass transport into the bulk (G_{bd} limiting case).

In the particle-phase regime, the classification step is based on SSR or the bulk saturation ratio (BSR) to distinguish between systems in the reaction-diffusion regime or the mass-transfer regime (Berkemeier et al., 2013). The BSR is defined analogously to SSR as the ratio of near-surface bulk concentration of an oxidation product to its saturation concentration.

B3 Criterion 3: Mixing Parameters (MP)

Is SOA growth limited by diffusion in the gas or particle phase? Depending on the reaction location and saturation ratio, mixing parameters are used to assess the heterogeneity of the gas-particle system. One can define the surface mixing parameter

ACPD
14, 5929–5961, 2014

(SMP), the bulk mixing parameter (BMP), the gas-phase diffusion correction factor (C_g), and the gas-particle mixing parameter (GMP). SMP is defined as the ratio of the actual surface concentration of compound i to the maximum possible surface concentration in the case of perfect particle-phase mixing. BMP is defined using an effective reacto-diffusive length (Berkemeier et al., 2013). As a MP approaches zero, a strong concentration gradient exists and the system is limited by diffusion; as MP approaches unity, the system is well-mixed and limited by reaction.

In mass-transfer limited systems (indicated by a low SR), $C_{g,i}$ distinguishes between gas-phase diffusion limitation and accommodation limitation. $C_{g,i}$ is defined as the ratio of the concentration of compound i in the near-surface gas phase (one mean free path away from the surface) to that in the gas phase far from the particle (Pöschl et al., 2007):

$$C_{g,i} = C_i^{gs}/C_i^{g} \tag{B4}$$

As $C_{g,i}$ approaches zero, the compound i exhibits a strong concentration gradient in the gas phase and the system is classified as gas-phase diffusion limited (G_{gd} limiting case); as $C_{g,i}$ approaches unity, the system is designated as accommodation-limited (G_α limiting case).

The gas-particle mixing parameter (GMP) is defined as the ratio of equilibrium gas-phase mass concentration of compound i, $C_i^{g,\,eq}$, to gas-phase mass concentration in the gas phase, C_i^{g} (far from particle):

$$\mathrm{GMP}_i = C_i^{g,\,eq}/C_i^{g} \tag{B5}$$

$C_i^{g,\,eq}$ can be calculated using an equilibrium partitioning theory (Pankow, 1994; Donahue et al., 2006):

$$C_i^{g,\,eq} = C_i^{*} \quad C_i^{PM}/C_{Tot} \tag{B6}$$

ACPD
14, 5929–5961, 2014

where C_i^* is the effective saturation mass concentration of compound i, C_i^{PM} is the particle mass concentration of compound i, and C_{Tot} is the total particle mass concentration. In the case of ideal mixing, C_i^* is equal to the gas-phase saturation mass concentration over the pure subcooled liquid (C_i^0). Note that $C_i^{g,\,eq}$ can be regarded as a gas-phase mass concentration just above the particle surface, C_i^s when Raoult's law is strictly obeyed and C_i^s is in equilibrium with the whole particle.

The value of GMP determines the extent to which SOA growth is controlled by quasi-equilibrium growth or limited by mass transfer. $C_i^g = C_i^s$ at gas-particle equilibrium. The particle still grows, if C_i^g changes slowly and C_i^s follows C_i^g instantaneously (quasi-equilibrium growth) (Shiraiwa and Seinfeld, 2012; Zhang et al., 2012). If $C_i^g > C_i^s$, compound i will diffuse from the gas to the particulate phase, driven by concentration or partial pressure gradient between the gas and particle phases (non-equilibrium or kinetically-limited growth). Thus, the numerical interpretation of GMP is: (1) As GMP approaches 0, SOA growth is limited kinetically by mass transfer; (2) As GMP approaches unity, SOA growth is in quasi-equilibrium and the system is subject to the gas-phase reaction limitation case G_{rx}.

Note that GMP is small for the limiting cases of G_{bd}, G_α, and G_{gd}. Interfacial transport comprises gas-phase diffusion, surface accommodation, and surface-to-bulk transport processes. Gas-phase diffusion and surface accommodation limitation can be differentiated from surface-to-bulk transport limitation either by SSR or by comparing surface (α_s) and bulk (α_b) accommodation coefficients, each of which is resolved by KM-GAP. α_s is defined as the probability of a molecule sticking to the surface upon collision, whereas α_b is defined as the respective probability of a molecule to enter the bulk of the particle (Pöschl et al., 2007; Shiraiwa et al., 2012). If $\alpha_s \approx \alpha_b$, then interfacial transport is not limited by surface-to-bulk exchange and thus is limited by either gas-phase diffusion or surface accommodation; if $\alpha_s > \alpha_b$, then the interfacial transport is limited by surface-to-bulk transport, (dissolution or bulk diffusion). For additional discussion of accommodation vs. surface-bulk exchange see Appendix C in Berkemeier et al. (2013).

ACPD
14, 5929–5961, 2014

Appendix C

Examples of kinetic regimes and limiting cases

Here we use KM-GAP to model condensation of a semi-volatile compound generated by oxidation of a parent VOC. We assume that the parent VOC with an initial concentration of $10^{10}\,cm^{-3}$ is converted to a semi-volatile product with a first-order rate coefficient of $0.1\,min^{-1}$. Conversion of the first-generation product to higher generation products and particle-phase reactions need not be considered. The initial number and mass concentrations of non-volatile pre-existing particles are taken as $10^{3}\,cm^{-3}$ and $0.1\,\mu g\,m^{-3}$, respectively. The initial particle size distribution is assumed log-normal with mean diameter of 50 nm and a standard deviation of 1.5. The saturation mass concentration of the oxidation product is assumed to be $10^{3}\,\mu g\,m^{-3}$. The required kinetic parameters for the simulation are given in Table A2. Surface accommodation coefficient ($\alpha_{s,0}$), bulk diffusion coefficient (D_b), and gas-phase diffusion coefficient (D_g) are varied to illustrate the different kinetic regimes and limiting cases for SOA formation in the gas-phase regime.

Figure A4 shows the results of such simulation. The temporal evolution of mass concentration of the parent VOC (black), the oxidation product in the gas phase (solid blue), in the near-surface gas phase (one mean free path away from the surface; dotted blue), just above particle surface (dashed blue), and in the particle phase (red) are shown. In the simulation presented in Fig. A4a, SOA growth is limited by gas-phase diffusion up to ~ 10 s (G_{gd} limiting case), indicated by a low surface saturation ratio (SSR) and a low the gas-phase diffusion correction factor (C_g) ($C^g > C^{gs}$). The gas-phase concentration gradient vanishes within ~ 10 s ($C^g \approx C^{gs}$), and as C^g continues to increase due to the conversion of the parent VOC, C^s follows the change in C^g essentially instantaneously and C^P increases. In this case, the gas-phase rate of formation of the oxidation product controls particle growth corresponding to the limiting case of G_{rx} (so-called quasi-equilibrium growth) (Shiraiwa and Seinfeld, 2012; Zhang et al., 2012).

ACPD
14, 5929–5961, 2014

In the simulation presented in Fig. A4b with a relatively low surface accommodation coefficient of 10^{-3}, a steep concentration gradient exhibits between the gas phase and the particle surface ($C^{g} \approx C^{gs} > C^{s}$) during SOA growth. The system is limited by accommodation (G_{α}), as SSR is low but C_{g} is 1.

Figure A4c shows the corresponding results for particles in an amorphous semi-solid state with the low bulk diffusion coefficient of $10^{-17}\,cm^{2}\,s^{-1}$. In this case, particle growth is limited by surface-to-bulk transport (G_{bd}), as SSR is high and GMP is low. The bulk accommodation coefficient α_{b} is $\sim 10^{-5}$, much smaller than the surface accommodation coefficient α_{s}. Sensitivity studies with varying D_{b} reveal that when $D_{b} < 10^{-12}\,cm^{2}\,s^{-1}$ the timescales for surface-bulk exchange and bulk diffusion become longer than that of gas-phase diffusion and accommodation (Shiraiwa and Seinfeld, 2012). From the Stokes–Einstein relation, this value corresponds to a viscosity of $\sim 10^{4}$ Pa s, which is on the same order as the viscosity of α-pinene SOA at 40–70 % RH (Renbaum-Wolff et al., 2013). Thus, SOA growth can be limited by bulk diffusion at low RH; whereas surface accommodation becomes more important at high RH.

Appendix D

Application to chamber data: dodecane photooxidation

Here we apply the classification scheme to experimental data on SOA formation from oxidation of the C_{12} alkane, dodecane ($C_{12}H_{28}$) in the Caltech Environmental Chamber (Yee et al., 2012). 34 ppb dodecane was oxidized by OH radicals over 20 h in the presence of dry ammonium sulfate seed particles at low concentrations of NO_{x} typical of nonurban conditions. KM-GAP was used to simulate the evolution of SOA mass, the organic atomic oxygen-to-carbon (O : C) ratio, and particle-size distribution in the chamber experiments (Shiraiwa et al., 2013a). In the gas phase, SVOCs resulting from up to five generations of OH oxidation are considered. Some of the fourth generation products have been established to be multifunctional carbonyl compounds (aldehydes)

ACPD
14, 5929–5961, 2014

that can react in the particle phase with hydroperoxide, hydroxyl, and peroxycarboxylic acid groups, forming peroxyhemiacetal (PHA), hemiacetal, and acylperoxyhemiacetal, respectively (Docherty et al., 2005; Yee et al., 2012; Ziemann and Atkinson, 2012). The observed evolution of the particle size distribution is simulated successfully, only if such particle-phase chemistry is included (Shiraiwa et al., 2013a).

Figure A5a shows the span of O : C ratio and gas-phase saturation concentrations over the pure subcooled liquids (C_i^0) for gas-phase oxidation products and particle-phase products of the dodecane system. The smaller symbols indicate individual products predicted in the dodecane photooxidation chemical mechanism (Yee et al., 2012) and the large solid circles indicate the surrogate compounds used in the KM-GAP simulations (Shiraiwa et al., 2013a). Upon gas-phase multi-generation oxidation, the volatility of SVOCs decreases from $\sim 10^6\,\mu g\,m^{-3}$ (dodecane) to $\sim 1\,\mu g\,m^{-3}$. The particle-phase products have significantly lower volatilities of $\sim 10^{-2}\,\mu g\,m^{-3}$.

Figure A5b and c shows the temporal evolution of mass concentration of the 1st and 5th generation oxidation products in the gas phase (C^g), at the particle surface (C^s), and in the particle phase (C^P). C^g is slightly higher than C^s up to ~ 5 h due to continuous generation of oxidation products in the gas phase, and eventually reaching $C^g \approx C^s$ for both products (GMP ≈ 1). Note that mass concentration in the near surface gas phase (C^{gs}) is identical to C^g, indicating that gas-phase diffusion is not a limiting step. The same trend is seen for other generation products. Thus, the contribution of gas-phase semi-volatile oxidation products to SOA formation is limited by their formation in the gas phase, corresponding to the limiting case of G_{rx}.

Particle-phase products are formed by the reaction of reactive aldehydes with SVOCs in the particle phase. Simulations suggest that this reaction occurs mainly at the surface and in the near-surface bulk (Shiraiwa et al., 2013a). Aldehydes and SVOCs are both saturated in the bulk (BSR is high). A strong concentration gradient of aldehydes in the bulk is predicted, whereas SVOCs are predicted to be essentially homogeneous in the bulk ($BMP_{XY} \approx 0.5$). Bulk reaction is tightly coupled with bulk diffusion and the system falls into the reaction-diffusion regime (B^{rd}), particularly the tra-

ACPD
14, 5929–5961, 2014

ditional reacto-diffusive case (B^{rd}_{trad}) (Worsnop et al., 2002; Pöschl et al., 2007; Kolb et al., 2010; Berkemeier et al., 2013).

Acknowledgements. This work was funded by the Max Planck Society and US National Science Foundation grant AGS-1057183. M. Shiraiwa, T. Berkemeier, and U. Pöschl thank the European Commission project Pan-European gas-aerosols-climate interaction study (No. 265148, PEGASOS). MS thanks the Japan Society for the Promotion of Science (JSPS) for Postdoctoral Fellowships for Research Abroad.

The service charges for this open access publication have been covered by the Max Planck Society.

References

Berkemeier, T., Huisman, A. J., Ammann, M., Shiraiwa, M., Koop, T., and Pöschl, U.: Kinetic regimes and limiting cases of gas uptake and heterogeneous reactions in atmospheric aerosols and clouds: a general classification scheme, Atmos. Chem. Phys., 13, 6663–6686, doi:10.5194/acp-13-6663-2013, 2013.

Chang, E. I. and Pankow, J. F.: Prediction of activity coefficients in liquid aerosol particles containing organic compounds, dissolved inorganic salts, and water – Part 2: Consideration of phase separation effects by an X-UNIFAC model, Atmos. Environ., 40, 6422–6436, 2006.

Compernolle, S., Ceulemans, K., and Müller, J.-F.: EVAPORATION: a new vapour pressure estimation methodfor organic molecules including non-additivity and intramolecular interactions, Atmos. Chem. Phys., 11, 9431–9450, doi:10.5194/acp-11-9431-2011, 2011.

Crounse, J. D., Nielsen, L. B., Jørgensen, S., Kjaergaard, H. G., and Wennberg, P. O.: Autoxidation of organic compounds in the atmosphere, J. Phys. Chem. Lett., 4, 3513–3520, 2013.

Docherty, K. S., Wu, W., Lim, Y. B., and Ziemann, P. J.: Contributions of organic peroxides to secondary aerosol formed from reactions of monoterpenes with O_3, Environ. Sci. Technol., 39, 4049–4059, 2005.

Donahue, N. M., Robinson, A. L., Stanier, C. O., and Pandis, S. N.: Coupled partitioning, dilution, and chemical aging of semivolatile organics, Environ. Sci. Technol., 40, 2635–2643, 2006.

ACPD
14, 5929–5961, 2014

Donahue, N. M., Epstein, S. A., Pandis, S. N., and Robinson, A. L.: A two-dimensional volatility basis set: 1. organic-aerosol mixing thermodynamics, Atmos. Chem. Phys., 11, 3303–3318, doi:10.5194/acp-11-3303-2011, 2011.

Donahue, N. M., Henry, K. M., Mentel, T. F., Kiendler-Scharr, A., Spindler, C., Bohn, B., Brauers, T., Dorn, H. P., Fuchs, H., Tillmann, R., Wahner, A., Saathoff, H., Naumann, K.-H., Möhler, O., Leisner, T., Müller, L., Reinnig, M.-C., Hoffmann, T., Salo, K., Hallquist, M., Frosch, M., Bilde, M., Tritscher, T., Barmet, P., Praplan, A. P., DeCarlo, P. F., Dommen, J., Prévôt, A. S. H., and Baltensperger, U.: Aging of biogenic secondary organic aerosol via gas-phase OH radical reactions, P. Natl. Acad. Sci. USA, 109, 13503–13508, 2012.

Ervens, B., Turpin, B. J., and Weber, R. J.: Secondary organic aerosol formation in cloud droplets and aqueous particles (aqSOA): a review of laboratory, field and model studies, Atmos. Chem. Phys., 11, 11069–11102, doi:10.5194/acp-11-11069-2011, 2011.

Goldstein, A. H. and Galbally, I. E.: Known and unexplored organic constituents in the earth's atmosphere, Environ. Sci. Technol., 41, 1514–1521, 2007.

Hallquist, M., Wenger, J. C., Baltensperger, U., Rudich, Y., Simpson, D., Claeys, M., Dommen, J., Donahue, N. M., George, C., Goldstein, A. H., Hamilton, J. F., Herrmann, H., Hoffmann, T., Iinuma, Y., Jang, M., Jenkin, M. E., Jimenez, J. L., Kiendler-Scharr, A., Maenhaut, W., McFiggans, G., Mentel, Th. F., Monod, A., Prévôt, A. S. H., Seinfeld, J. H., Surratt, J. D., Szmigielski, R., and Wildt, J.: The formation, properties and impact of secondary organic aerosol: current and emerging issues, Atmos. Chem. Phys., 9, 5155–5236, doi:10.5194/acp-9-5155-2009, 2009.

Hosny, N. A., Fitzgerald, C., Tong, C., Kalberer, M., Kuimova, M. K., and Pope, F. D.: Fluorescent lifetime imaging of atmospheric aerosols: a direct probe of aerosol viscosity, Faraday Discuss., 165, 343–356, 2013.

Jang, M. S., Czoschke, N. M., Lee, S., and Kamens, R. M.: Heterogeneous atmospheric aerosol production by acid-catalyzed particle-phase reactions, Science, 298, 814–817, 2002.

Jaoui, M., Corse, E., Kleindienst, T. E., Offenberg, J. H., Lewandowski, M., and Edney, E. O.: Analysis of secondary organic aerosol compounds from the photooxidation of *d*-limonene in the presence of NO_x and their detection in ambient $PM_{2.5}$, Environ. Sci. Technol., 40, 3819–3828, 2006.

Jimenez, J. L., Canagaratna, M. R., Donahue, N. M., Prevot, A. S. H., Zhang, Q., Kroll, J. H., DeCarlo, P. F., Allan, J. D., Coe, H., Ng, N. L., Aiken, A. C., Docherty, K. S., Ulbrich, I. M., Grieshop, A. P., Robinson, A. L., Duplissy, J., Smith, J. D., Wilson, K. R., Lanz, V. A.,

ACPD
14, 5929–5961, 2014

Hueglin, C., Sun, Y. L., Tian, J., Laaksonen, A., Raatikainen, T., Rautiainen, J., Vaattovaara, P., Ehn, M., Kulmala, M., Tomlinson, J. M., Collins, D. R., Cubison, M. J., Dunlea, E. J., Huffman, J. A., Onasch, T. B., Alfarra, M. R., Williams, P. I., Bower, K., Kondo, Y., Schneider, J., Drewnick, F., Borrmann, S., Weimer, S., Demerjian, K., Salcedo, D., Cottrell, L., Griffin, R., Takami, A., Miyoshi, T., Hatakeyama, S., Shimono, A., Sun, J. Y., Zhang, Y. M., Dzepina, K., Kimmel, J. R., Sueper, D., Jayne, J. T., Herndon, S. C., Trimborn, A. M., Williams, L. R., Wood, E. C., Middlebrook, A. M., Kolb, C. E., Baltensperger, U., and Worsnop, D. R.: Evolution of organic aerosols in the atmosphere, Science, 326, 1525–1529, 2009.

Kalberer, M., Sax, M., and Samburova, V.: Molecular size evolution of oligomers in organic aerosols collected in urban atmospheres and generated in a smog chamber, Environ. Sci. Technol., 40, 5917–5922, 2006.

Kolb, C. E., Cox, R. A., Abbatt, J. P. D., Ammann, M., Davis, E. J., Donaldson, D. J., Garrett, B. C., George, C., Griffiths, P. T., Hanson, D. R., Kulmala, M., McFiggans, G., Pöschl, U., Riipinen, I., Rossi, M. J., Rudich, Y., Wagner, P. E., Winkler, P. M., Worsnop, D. R., and O' Dowd, C. D.: An overview of current issues in the uptake of atmospheric trace gases by aerosols and clouds, Atmos. Chem. Phys., 10, 10561–10605, doi:10.5194/acp-10-10561-2010, 2010.

Koop, T., Bookhold, J., Shiraiwa, M., and Pöschl, U.: Glass transition and phase state of organic compounds: dependency on molecular properties and implications for secondary organic aerosols in the atmosphere, Phys. Chem. Chem. Phys., 13, 19238–19255, 2011.

Kroll, J. H. and Seinfeld, J. H.: Chemistry of secondary organic aerosol: formation and evolution of low-volatility organics in the atmosphere, Atmos. Environ., 42, 3593–3624, 2008.

Kundu, S., Fisseha, R., Putman, A. L., Rahn, T. A., and Mazzoleni, L. R.: High molecular weight SOA formation during limonene ozonolysis: insights from ultrahigh-resolution FT-ICR mass spectrometry characterization, Atmos. Chem. Phys., 12, 5523–5536, doi:10.5194/acp-12-5523-2012, 2012.

Kuwata, M. and Martin, S. T.: Phase of atmospheric secondary organic material affects its reactivity, P. Natl. Acad. Sci. USA, 109, 17354–17359, 2012.

Lim, Y. B., Tan, Y., Perri, M. J., Seitzinger, S. P., and Turpin, B. J.: Aqueous chemistry and its role in secondary organic aerosol (SOA) formation, Atmos. Chem. Phys., 10, 10521–10539, doi:10.5194/acp-10-10521-2010, 2010.

ACPD
14, 5929–5961, 2014

Loza, C. L., Craven, J. S., Yee, L. D., Coggon, M. M., Schwantes, R. H., Shiraiwa, M., Zhang, X., Schilling, K. A., Ng, N. L., Canagaratna, M. R., Ziemann, P. J., Flagan, R. C., and Seinfeld, J. H.: Secondary organic aerosol yields of 12-carbon alkanes, Atmos. Chem. Phys. Discuss., 13, 20677–20727, doi:10.5194/acpd-13-20677-2013, 2013.

Pankow, J. F.: An absorption-model of the gas aerosol partitioning involved in the formation of secondary organic aerosol, Atmos. Environ., 28, 189–193, 1994.

Perraud, V., Bruns, E. A., Ezell, M. J., Johnson, S. N., Yu, Y., Alexander, M. L., Zelenyuk, A., Imre, D., Chang, W. L., Dabdub, D., Pankow, J. F., and Finlayson-Pitts, B. J.: Nonequilibrium atmospheric secondary organic aerosol formation and growth, P. Natl. Acad. Sci. USA, 109, 2836–2841, 2012.

Pöschl, U., Rudich, Y., and Ammann, M.: Kinetic model framework for aerosol and cloud surface chemistry and gas-particle interactions – Part 1: General equations, parameters, and terminology, Atmos. Chem. Phys., 7, 5989–6023, doi:10.5194/acp-7-5989-2007, 2007.

Renbaum-Wolff, L., Grayson, J. W., Bateman, A. P., Kuwata, K., Sellier, M., Murray, B. J., Schilling, J. E., Martin, S. T., and Bertram, A. K.: Viscosity of α-pinene secondary organic material and implications for particle growth and reactivity, P. Natl. Acad. Sci. USA, 110, 8014–8019, 2013.

Riipinen, I., Pierce, J. R., Yli-Juuti, T., Nieminen, T., Häkkinen, S., Ehn, M., Junninen, H., Lehtipalo, K., Petäjä, T., Slowik, J., Chang, R., Shantz, N. C., Abbatt, J., Leaitch, W. R., Kerminen, V.-M., Worsnop, D. R., Pandis, S. N., Donahue, N. M., and Kulmala, M.: Organic condensation: a vital link connecting aerosol formation to cloud condensation nuclei (CCN) concentrations, Atmos. Chem. Phys., 11, 3865–3878, doi:10.5194/acp-11-3865-2011, 2011.

Shiraiwa, M. and Seinfeld, J. H.: Equilibration timescale of atmospheric secondary organic aerosol partitioning, Geophys. Res. Lett., 39, L24801, doi:10.1029/2012GL054008, 2012.

Shiraiwa, M., Ammann, M., Koop, T., and Pöschl, U.: Gas uptake and chemical aging of semisolid organic aerosol particles, P. Natl. Acad. Sci. USA, 108, 11003–11008, 2011.

Shiraiwa, M., Pfrang, C., Koop, T., and Pöschl, U.: Kinetic multi-layer model of gas-particle interactions in aerosols and clouds (KM-GAP): linking condensation, evaporation and chemical reactions of organics, oxidants and water, Atmos. Chem. Phys., 12, 2777–2794, doi:10.5194/acp-12-2777-2012, 2012.

Shiraiwa, M., Yee, L. D., Schilling, K. A., Loza, C. L., Craven, J. S., Zuend, A., Ziemann, P. J., and Seinfeld, J. H.: Size distribution dynamics reveal particle-phase chemistry in organic aerosol formation, P. Natl. Acad. Sci. USA, 110, 11746–11750, 2013a.

ACPD
14, 5929–5961, 2014

Shiraiwa, M., Zuend, A., Bertram, A. K., and Seinfeld, J. H.: Gas-particle partitioning of atmospheric aerosols: interplay of physical state, non-ideal mixing and morphology, Phys. Chem. Chem. Phys., 15, 11441–11453, 2013b.

Surratt, J. D., Murphy, S. M., Kroll, J. H., Ng, N. L., Hildebrandt, L., Sorooshian, A., Szmigielski, R., Vermeylen, R., Maenhaut, W., Claeys, M., Flagan, R. C., and Seinfeld, J. H.: Chemical composition of secondary organic aerosol formed from the photooxidation of isoprene, J. Phys. Chem. A, 110, 9665–9690, 2006.

Surratt, J. D., Chan, A. W. H., Eddingsaas, N. C., Chan, M. N., Loza, C. L., Kwan, A. J., Hersey, S. P., Flagan, R. C., Wennberg, P. O., and Seinfeld, J. H.: Reactive intermediates revealed in secondary organic aerosol formation from isoprene, P. Natl. Acad. Sci. USA, 107, 6640–6645, 2010.

Vaden, T. D., Imre, D., Beranek, J., Shrivastava, M., and Zelenyuk, A.: Evaporation kinetics and phase of laboratory and ambient secondary organic aerosol, P. Natl. Acad. Sci. USA, 108, 2190–2195, 2011.

Virtanen, A., Joutsensaari, J., Koop, T., Kannosto, J., YliPirilä, P., Leskinen, J., Mäkelä, J. M., Holopainen, J. K., Pöschl, U., Kulmala, M., Worsnop, D. R., and Laaksonen, A.: An amorphous solid state of biogenic secondary organic aerosol particles, Nature, 467, 824–827, 2010.

Vogel, A. L., Äijälä, M., Corrigan, A. L., Junninen, H., Ehn, M., Petäjä, T., Worsnop, D. R., Kulmala, M., Russell, L. M., Williams, J., and Hoffmann, T.: In situ submicron organic aerosol characterization at a boreal forest research station during HUMPPA-COPEC 2010 using soft and hard ionization mass spectrometry, Atmos. Chem. Phys., 13, 10933–10950, doi:10.5194/acp-13-10933-2013, 2013.

Williams, B. J., Goldstein, A. H., Kreisberg, N. M., and Hering, S. V.: In situ measurements of gas/particle-phase transitions for atmospheric semivolatile organic compounds, P. Natl. Acad. Sci. USA, 107, 6676–6681, 2010.

Worsnop, D. R., Morris, J. W., Shi, Q., Davidovits, P., and Kolb, C. E.: A chemical kinetic model for reactive transformations of aerosol particles, Geophys. Res. Lett., 29, 1–4,doi:10.1029/2002gl015542, 2002.

Yee, L. D., Craven, J. S., Loza, C. L., Schilling, K. A., Ng, N. L., Canagaratna, M. R., Ziemann, P. J., Flagan, R. C., and Seinfeld, J. H.: Secondary organic aerosol formation from low-NO_x photooxidation of dodecane: evolution of multigeneration gas-phase chemistry and aerosol composition, J. Phys. Chem. A, 116, 6211–6230, 2012.

ACPD
14, 5929–5961, 2014

Zhang, X., Pandis, S. N., and Seinfeld, J. H.: Diffusion-limited versus quasi-equilibrium aerosol growth, Aerosol Sci. Tech., 46, 874–885, 2012.
Ziemann, P. J. and Atkinson, R.: Kinetics, products, and mechanisms of secondary organic aerosol formation, Chem. Soc. Rev., 41, 6582–6605, 2012.
Zuend, A. and Seinfeld, J. H.: Modeling the gas-particle partitioning of secondary organic aerosol: the importance of liquid-liquid phase separation, Atmos. Chem. Phys., 12, 3857–3882, doi:10.5194/acp-12-3857-2012, 2012.

ACPD
14, 5929–5961, 2014

Table A1. Summary of analysis of identified SOA oxidation products. Number of identified oxidation products N, average molar mass M_{ave}, slope of fitted lines in Fig. 2 of molar mass vs. logarithm of volatility, coefficients of determination R^2 as well as R^2 for O : C vs. volatility.

precursor	oxidants	N	M_{ave} ($g\,mol^{-1}$)	slope ($g\,mol^{-1}$)	R^2 (molar mass)	R^2 (O : C)
isoprene	OH	26	350*	15 (±1)	0.87	0.09
α-pinene	O_3	37	400*	19 (±1)	0.86	0.28
limonene	OH, O_3	17	–	19 (±2)	0.87	0.38
dodecane	OH, low NO	116	429	25 (±1)	0.90	0.22
	OH, high NO	106	495	24 (±1)	0.84	0.29
cyclododecane	OH, low NO	77	384	18 (±1)	0.63	0.08
	OH, high NO	122	458	24 (±1)	0.78	0.08
hexylcyclohexane	OH, low NO	137	310	19 (±1)	0.60	0.05
	OH, high NO	230	418	20 (±1)	0.69	0.00

* (Kalberer et al., 2006)

ACPD
14, 5929–5961, 2014

Table A2. Properties and kinetic parameters of the VOC oxidation product used in the simulations for SOA growth.

Parameter (Unit)	Description	(a)	(b)	(c)
$\alpha_{s,0}$	surface accommodation coefficient	1	10^{-3}	1
τ_d(s)	desorption lifetime	10^{-6}	10^{-6}	10^{-6}
D_b ($cm^2\ s^{-1}$)	bulk diffusion coefficient	10^{-5}	10^{-5}	10^{-17}
D_g ($cm^2\ s^{-1}$)	gas-phase diffusion coefficient	0.01	0.05	0.05
k_g (min^{-1})	first-order gas-phase reaction rate coefficient	0.1	0.1	0.1

ACPD
14, 5929–5961, 2014

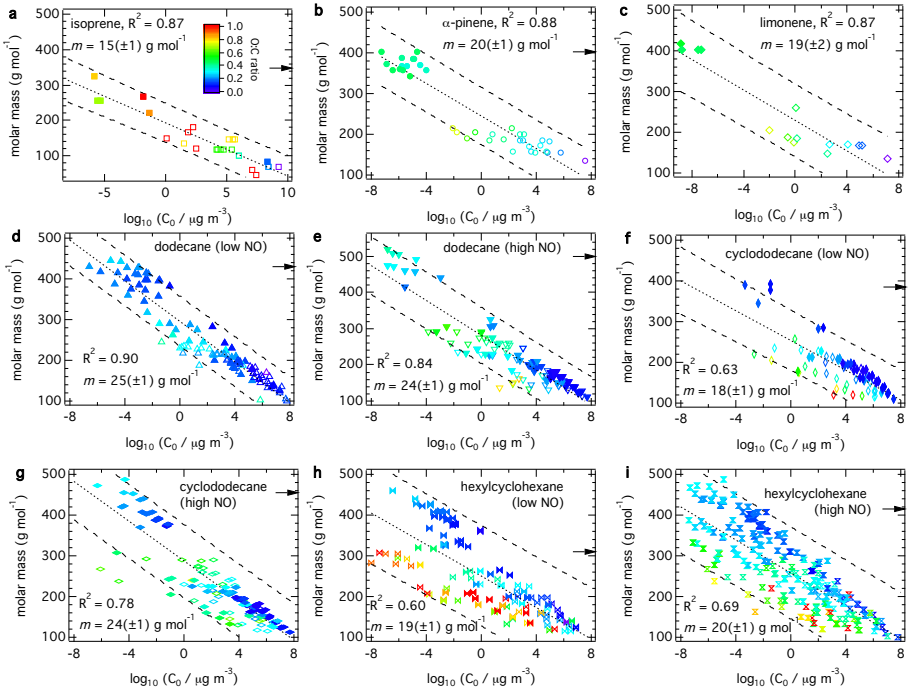

Fig. 1. Molecular corridors of SOA evolution in various SOA systems. Molar mass vs. volatility (C_0) at 298 K for oxidation products of isoprene **(a)**, α-pinene **(b)**, limonene **(c)**, dodecane at low **(d)** and high **(e)** NO condition, cyclododecane at low **(f)** and high **(g)** NO condition, and hexylcyclohexane at low **(h)** and high **(i)** NO condition. The open and solid markers correspond to the gas- and particle-phase products, respectively, color-coded by atomic O : C ratio. With a linear regression analysis, the coefficient of determination (R^2), fitted lines (dotted lines) and their slopes (m), and prediction intervals with 95 % confidence (dashed lines) are shown. The arrows on the right axis indicate average molar mass for isoprene and α-pinene (Kalberer et al., 2006) as well as for alkanes as measured in this study.

ACPD
14, 5929–5961, 2014

Molecular corridors represent the multiphase chemical evolution of SOA

M. Shiraiwa et al.

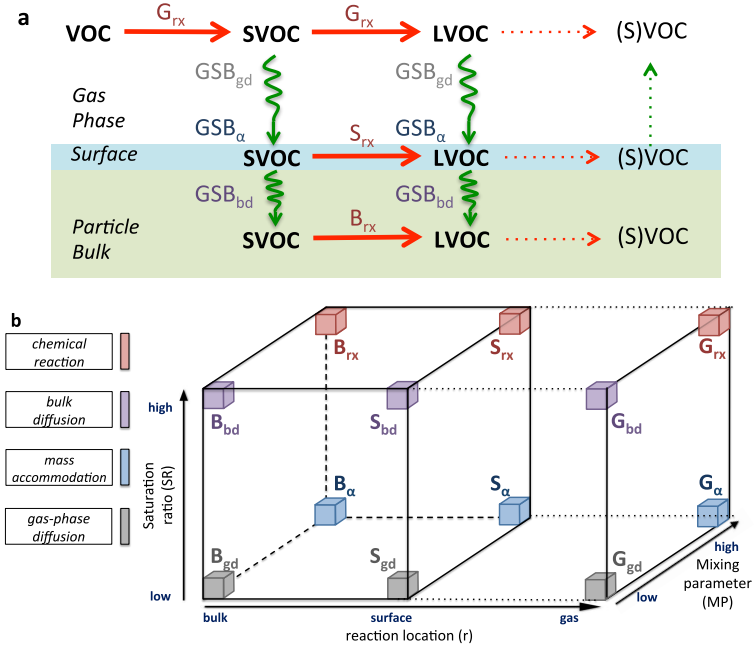

Fig. 2. Kinetic regimes of SOA formation and aging. **(a)** Schematic outline of the formation and aging of secondary organic aerosol. Red and green arrows denote chemical reactions and mass transport, respectively. Sequential and parallel reactions in the gas phase, at the particle surface, and in the particle bulk lead to multiple generations of semi- and low-volatility oxidation products (SVOC, LVOC). Dashed arrows denote revolatilization resulting from fragmentation reactions. **(b)** Kinetic regimes of SOA formation and aging are mapped onto the axes of a cuboid representing reaction location, saturation ratio, and mixing parameter. The horizontal axes from left to right correspond to four regimes governed by chemical reaction (red), bulk diffusion (purple), mass accommodation (blue), or gas-phase diffusion (grey). Each of these regimes includes three distinct cases characterized by a single rate-limiting process and a dominant reaction location.

ACPD
14, 5929–5961, 2014

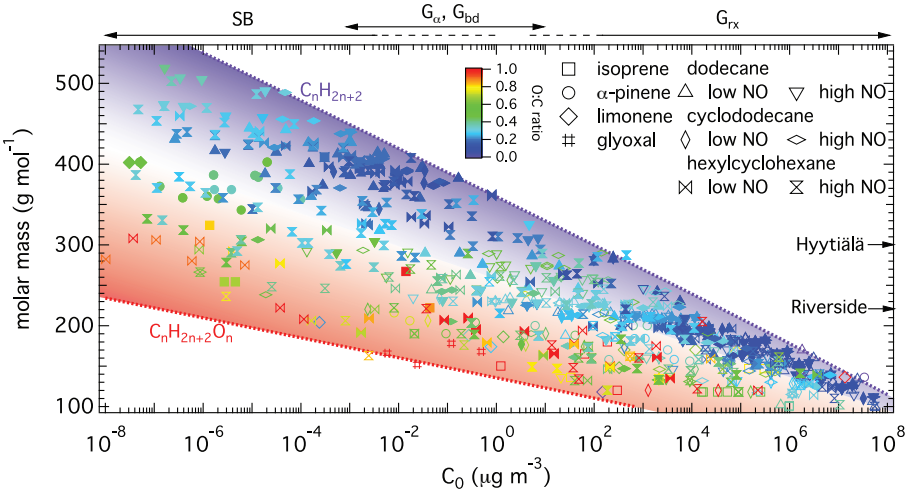

Fig. 3. Molecular corridors and kinetic regimes of SOA evolution. Molar mass vs. volatility (C_0) at 298 K for gas-phase (open) and particle-phase (solid) oxidation products of isoprene, α-pinene, limonene, glyoxal, dodecane, cyclododecane, and hexylcyclohexane. The dotted lines represent linear alkanes C_nH_{2n+2} (purple with O : C = 0) and sugar alcohols $C_nH_{2n+2}O_n$ (red with O : C = 1). Relevant kinetic regimes are indicated on the top of the plot. The split of molecular corridors between high and low O : C compounds (HOC, red shaded area; LOC, blue shaded area) reflects the median correlation fitted lines from Fig. 1. The arrows on the right axis indicate average molar masses of ambient SOA at Hyytiälä, Finland (Vogel et al., 2013) and at Riverside, California (Williams et al., 2010).

ACPD
14, 5929–5961, 2014

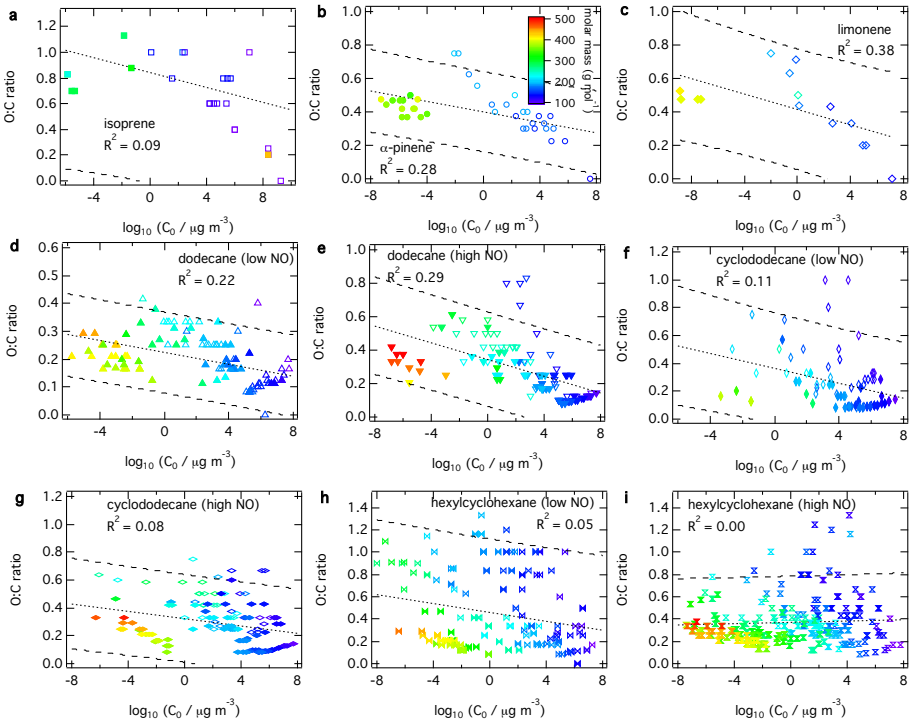

Fig. A1. Atomic O : C ratio vs. volatility (C_0) at 298 K for oxidation products of isoprene **(a)**, α-pinene **(b)**, limonene **(c)**, dodecane at low **(d)** and high **(e)** NO condition, cyclododecane under low **(f)** and high **(g)** NO conditions, and hexylcyclohexane at low **(h)** and high **(i)** NO conditions. The solid and open markers, color-coded with molar mass (g mol^{-1}), correspond to the gas- and particle-phase products, respectively. With a linear regression analysis, the correlation between both quantities has been evaluated (dotted lines) with coefficients of determination (R^2), including prediction intervals at the 95 % confidence level (dashed lines).

ACPD
14, 5929–5961, 2014

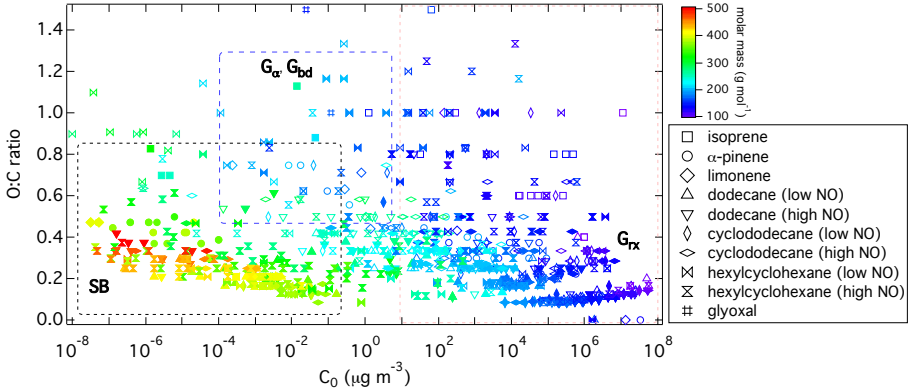

Fig. A2. Summary of O : C ratio vs. C_0 for isoprene, α-pinene, dodecane, limonene, dodecane, cyclododecane, hyxylcyclohexane, and glyoxal. The solid and open markers, color-coded with molar mass (g mol^{-1}), correspond to the gas- and particle-phase products, respectively. The possible kinetic regimes and limiting cases are depicted with dashed boxes.

ACPD
14, 5929–5961, 2014

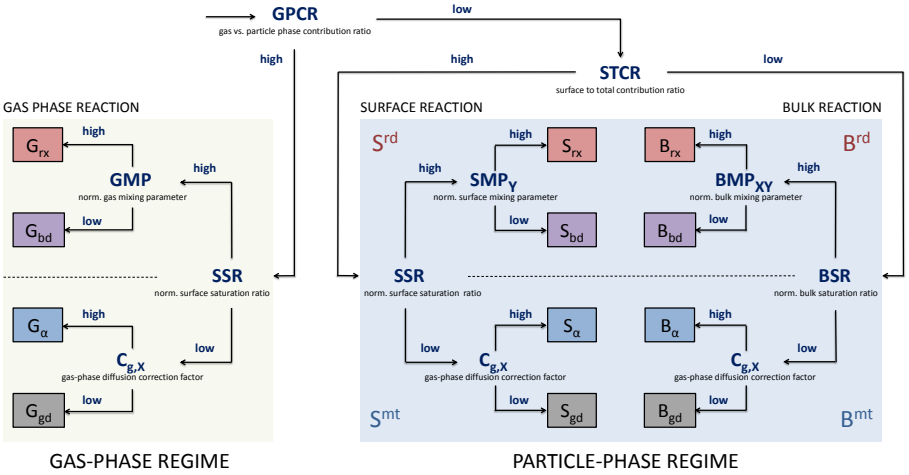

Fig. A3. Decision tree for classification and distinction of limiting cases for multiphase chemical evolution of SOA. The classification is based on: (1) the location of the reaction leading to its formation, (2) its saturation ratio, and (3) its mixing parameter to assess the heterogeneity in the gas and particle phases. The resulting limiting cases are shown in the small boxes with reaction location in the gas phase (G), at the surface (S) and in the bulk (B) and limiting processes of chemical reaction (rx), bulk diffusion (bd), mass accommodation (α), and gas-phase diffusion (gd).

ACPD
14, 5929–5961, 2014

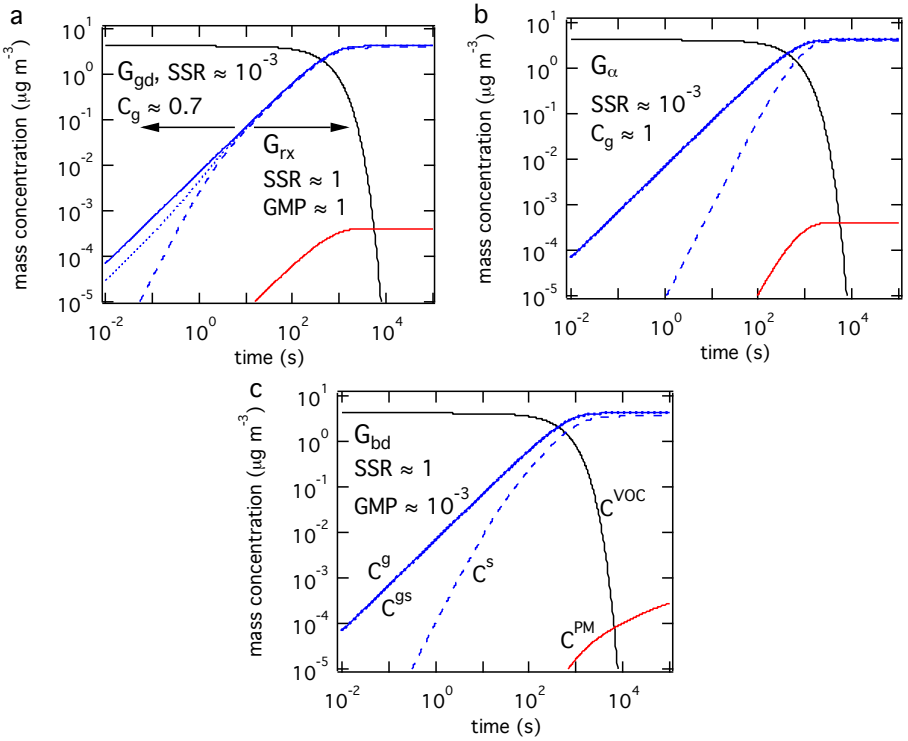

Fig. A4. Temporal evolution of mass concentration of the hypothesized VOC oxidation product in the gas phase (solid blue), in the near-surface gas phase (dotted blue), just above particle surface (dashed blue), and in the particle phase (red). The gas-phase mass concentration of the parent VOC is shown by the black line. SOA growth is limited **(a)** by gas-phase diffusion (G_{gd}) and reaction (G_{rx}), **(b)** by accommodation (G_{α}), and **(c)** bulk diffusion (G_{bd}).

ACPD
14, 5929–5961, 2014

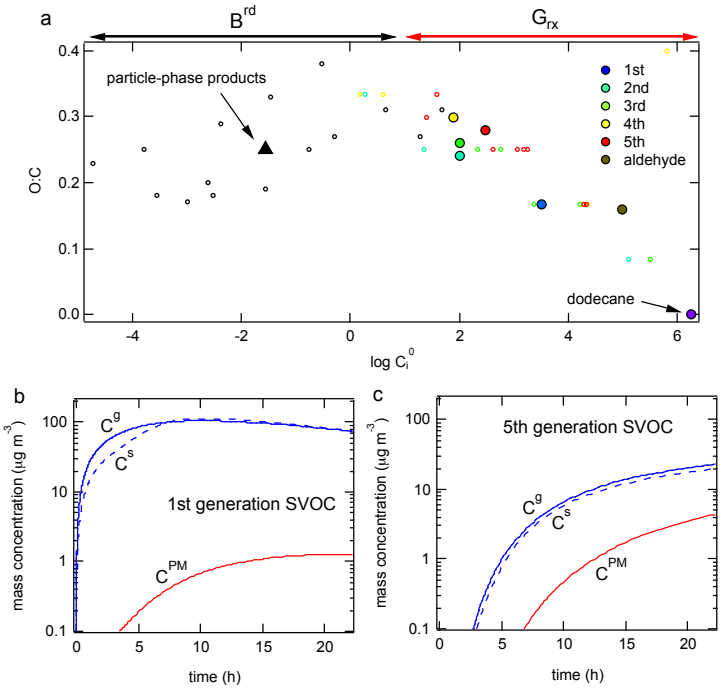

Fig. A5. Modeling SOA formation from dodecane photooxidation. **(a)** O : C ratios for products of dodecane oxidation vs. their predicted gas-phase saturation concentration ($\mu g\,m^{-3}$) (C_i^0) (adapted from Shiraiwa et al., 2013a). The smaller symbols indicate individual products predicted in the dodecane photooxidation chemical mechanism (Yee et al., 2012). Color indicates the gas-phase generation in which the compound is formed, including reactive carbonyl compounds. Black symbols indicate particle-phase products. The large solid circles indicate the surrogate SVOC compounds used in the KM-GAP simulations. Kinetic regimes of oxidation products are indicated on the top axis. **(b, c)** Temporal evolution of mass concentration of the **(b)** 1st and **(c)** 5th generation products in the gas phase (solid blue), just above particle surface (dashed blue), and in the particle phase (red).

ACPD
14, 5929–5961, 2014